Synthesis of cholic acid-core (ε-caprolactone-ran-lactide)-b-poly(ethylene glycol) 1000 random copolymer as chemotherapeutic nanocarriers for liver cancer treatment

Journal:	*Biomaterials Science*
Manuscript ID:	BM-ART-04-2014-000134
Article Type:	Paper
Date Submitted by the Author:	22-Apr-2014
Complete List of Authors:	Tao, Wei; Tsinghua University, Zeng, Xiaowei; Tsinghua University, Zhang, Jinxie; Tsinghua University, Zhu, Huijun; Tsinghua University, Chang, Danfeng; Tsinghua University, Zhang, Xudong; Tsinghua University, Gao, Yongfeng; Tsinghua University, Tang, Jiao; Tsinghua University, Huang, Laiqiang; Tsinghua University, Mei, Lin; Graduate School at Shenzhen, Tsinghua University,

SCHOLARONE™
Manuscripts

1   **Synthesis of cholic acid-core (*ε*-caprolactone-*ran*-lactide)-*b*-poly(ethylene glycol)**

2   **1000 random copolymer as chemotherapeutic nanocarriers for liver cancer**

3   **treatment**

4

5   Wei Tao[a,b,1], Xiaowei Zeng[a,b,1], Jinxie Zhang[a,b], Huijun Zhu[a,b], Danfeng Chang[b,c],

6   Xudong Zhang[a,b], Yongfeng Gao[a,b], Jiao Tang[d], Laiqiang Huang[a,b*], Lin Mei[a,b*]

7

8   [a] *School of Life Sciences, Tsinghua University, Beijing 100084, P.R. China*

9   [b] *The Ministry-Province Jointly Constructed Base for State Key Lab- Shenzhen Key*

10   *Laboratory of Chemical Biology, the Shenzhen Key Lab of Gene and Antibody*

11   *Therapy, and Division of Life and Health Sciences, Graduate School at Shenzhen,*

12   *Tsinghua University, Shenzhen 518055, P.R. China*

13   [c] *Department of Chemistry, Tsinghua University, Beijing 100084, P.R. China*

14   [d] *School of Medicine, Tsinghua University, Beijing 100084, P.R. China*

15

16   1, these authors contributted equally to this work.

17

18   [*]Corresponding author. Tel./Fax: +86 75526036736.

19   *E-mail address:* mei.lin@sz.tsinghua.edu.cn (L. Mei)

20   [*]Corresponding author. Tel./Fax: +86 75526036052

21   *E-mail address:* huanglq@sz.tsinghua.edu.cn (L. Huang).

22

1 **ABSTRACT**

2   A star-shaped random copolymer, cholic acid functionalized (ε-caprolactone

3 -*ran*-lactide)-*b*-poly(ethylene glycol) 1000 (CA-(PCL-*ran*-PLA)-*b*-PEG$_{1k}$), was

4 synthesized by a core-first approach through three parts of chemical reaction, and

5 characterized by hydrogen-1 nuclear magnetic resonance (^{1}H NMR), gel permeation

6 chromatography (GPC) and thermogravimetric analysis (TGA). The docetaxel-loaded

7 nanoparticles (NPs) were prepared by a modified nano-precipitation method. The

8 formation and characterization of these NPs were confirmed through dynamic light

9 scattering (DLS), zeta potential measurements, field emission scanning electron

10 microscopy (FESEM), and transmission electron microscopy (TEM). The *in vitro*

11 release profiles indicated that CA-(PCL-*ran*-PLA)-*b*-PEG$_{1k}$ NPs had an excellent

12 sustained and controlled drug release property. Both confocal laser scanning

13 microscope (CLSM) and flow cytometric (FCM) results showed the coumarin-6

14 loaded CA-(PCL-*ran*-PLA)-*b*-PEG$_{1k}$ NPs had the highest cellular uptake efficiency

15 compared with PEG$_{1k}$-*b*-(PCL-*ran*-PLA) NPs and CA-(PCL-*ran*-PLA) NPs in human

16 hepatic carcinoma cells. The docetaxel-loaded CA-(PCL-*ran*-PLA)-*b*-PEG$_{1k}$ NPs

17 were also proved to have the highest drug loading content, encapsulation efficiency,

18 and the best anti-tumor efficacy both *in vitro* and *in vivo*. In conclusion, the

19 star-shaped CA-(PCL-*ran*-PLA)-*b*-PEG$_{1k}$ copolymer was successfully synthesized

20 and could be used as a promising drug-loaded biomaterial for liver cancer

21 chemotherapy.

22

1. Introduction

It is reported that live cancer (hepatocellular carcinoma) has resulted in 754,000 deaths as of 2010 worldwide, making it the 3rd leading cause of cancer death after lung cancer and stomach cancer [1]. Current clinical treatments for liver cancer are mainly including surgery followed by radiotherapy, chemotherapy, and some emerging modalities (e.g. gene therapy, immunotherapy, phototherapy, and thermal therapy). However, each of these single modalities could hardly provide complete treatment because of their dose limitation and the resistance of cancer cells to the modality [2]. For example, chemotherapy is nonspecific and accompanied by side effects, due to lack of drug targeting, resistance of cancer cells and problems in permeability, solubility and stability of anticancer drugs [3].

Nanomedicine, the application of nanotechnology to medicine, has shown significant prospects solving these problems in cancer chemotherapy. Especially biodegradable polymeric NPs formulation, which could provide controlled and sustained delivery of anticancer drugs, is expected to fundamentally to change the landscape of pharmaceutical and biotechnology industries[4-6]. Due to the pathophysiological condition and anatomical changes caused by cancer, polymeric NPs designed for drug delivery system can be exploited for passively targeting of drugs [7]. Thus, an enhanced permeability and retention (EPR) effect of the polymeric NPs can be found in tumors as a result of the increased vascular permeability coupled with an impaired lymphatic drainage. Moreover, high drug loading capacity, high stability, excellent tolerability, protection of incorporated labile drugs from

1 degradation, controlled release and feasibility of variable routes of administration (e.g.

2 parenteral, oral, dermal, ocular, pulmonary, and rectal) are important technological

3 advantages brought by drug-loaded NPs [8]. Polymeric NPs could also reduce the

4 multidrug resistance characterized by many anti-cancer drugs (e.g. docetaxel) through

5 endocytosis of the drugs [9], and prevent drug efflux from cells mediated by the

6 P-glycoprotein [10]. Compared with conventional chemotherapy, polymeric NPs in

7 drug delivery system have advantages on overcoming annoying problems such as the

8 toxicity of drugs to normal tissues, limited aqueous solubility, short circulation

9 half-life in plasma and non-selectivity [11].

10 Biodegradable polymers approved by FDA, such as poly (ε-caprolactone) (PCL)

11 and poly(lactide) (PLA), are widely used in research of polymeric nanoformulations

12 nowadays [12-15]. PCL has attracted considerable interest owing to its permeability

13 to drugs, non-cytotoxicity, miscible properties with other polymers and

14 biocompatibility [16, 17]. However, PCL is easy to crystallize, which attenuates its

15 compatibility with soft tissues and makes it degrade much slower than PLA, thus

16 limiting the application of PCL in nanomedicine [18]. Nevertheless, this problem

17 could be settled through the copolymerization of ε-caprolactone with other monomers

18 [19, 20]. PLA is a thermoplastic aliphatic polyester and can be used as medical

19 implants for its biodegradable property [21, 22]. Copolymerization between lactide

20 enantiomers leading to PLA with variable stereoregularity, is a useful approach to

21 adjust degradability as well as mechanical and physical properties. It was reported

22 that PEGylation, chemical modification with poly(ethylene glycol) (PEG), is an

1   effective way to improve biological potencies of various pharmaceutical formulations

2   *in vivo* [23], and drugs conjugation to PEG or formulated in PEG copolymer

3   nanocarriers can enhance its solubility, permeability, stability and thus oral

4   bioavailability [24, 25]. Novel polymers with desired parameters between properties

5   of the parent polymers could be obtained by random copolymerization, which is

6   valuable for nanoparticle-based drug delivery system [26-28]. Cholic acid (CA),

7   composed of a steroid unit with three hydroxyl groups and one carboxyl group, is the

8   main bile acid in body. Due to its biological origin, CA was selected as the

9   polyhydroxy initiator, generating better biocompatibility for polymers incorporated

10   with CA moiety [2, 29]. Moreover, it is reported that CA functionalized copolymers

11   exhibited faster hydrolytic degradation rate compared with PCL, and the existence of

12   CA moiety in drug delivery system could also significantly enhance both cell

13   proliferation and adherence [30]. Branched polymers with useful rheological and

14   mechanical properties, such as star-shaped polymers, hyperbranched polymers and

15   dendrimers, have attracted a great deal of attention by research groups all over the

16   world [31-33]. With several branches extending from a single point [34], Star-shaped

17   polymers applied in drug carriers have advantages such as lower solution viscosity,

18   smaller hydrodynamic radius, encapsulation efficiency and higher loading content

19   compared with linear polymers in drug delivery system [32, 35-37]. Therefore,

20   star-shaped block copolymers based on PCL, PLA, PEG_{1k} and CA can provide

21   prospects for preparing excellent biodegradable drug-carriers [38, 39]. In this study,

22   we   successfully   synthesized   a   star-shaped   random   copolymer

1   CA-(PCL-*ran*-PLA)-*b*-PEG$_{1k}$ with three branch arms for docetaxel (DTX) delivery.

2   The DTX-loaded NPs exhibited satisfactory drug loading content, encapsulation

3   efficiency, and achieved significant *in vivo* therapeutic effects for liver cancer

4   treatment.

5

6   2. Materials and methods

7   2.1 Materials

8   *Agents:* D,L-lactide (3,6-dimethyl-1,4-dioxane-2,5-dione, $C_6H_8O_4$), cholic acid

9   (CA), 1,3-diisopropylcarbodiimide (DCC), and 4-(dimethylamino)pyridine (DMAP)

10   were purchased from Sigma (St. Louis, MO, USA). ε-caprolactone (CL) was obtained

11   from Acros Organics (Geel, Belgium). Poly(ethylene glycol) (PEG M_n 1000) was

12   purchased from   Shanghai Yare Biotech, Inc. (Shanghai, China). DTX and

13   commercial Taxotere[®] were provided by Shanghai Jinhe Bio-tech Co., Ltd. (Shanghai,

14   China).   Stannous   octoate $(Sn(Oct)_2)$ and

15   3-(4,5-Dimethylthiazol-2-yl)-2,5-Diphenyltetrazolium Bromide (MTT) were supplied

16   by Sigma (St. Louis, MO, USA). Acetonitrile and methanol were obtained from EM

17   Science (ChromAR, HPLC grade, Mallinckrodt Baker, USA). All other agents used

18   were of analytical reagent grade. Ultrahigh pure water utilised throughout all

19   experiments was produced by Boon Environmental Tech. Industry Co., Ltd. (Tianjin,

20   China)**.**

21   *Cells and Animals:* HepG2 cells (Human liver carcinoma cell line) were from

22   American Type Culture Collection (ATCC, Rockville, MD, USA). The female severe

1   combined immunodeficient (SCID) mice were purchased from the Institute of

2   Laboratory Animal Sciences, Chinese Academy of Medical Science. All the protocols

3   for the proposed human cancer cell lines and animal experiments were approved by

4   the Administrative Committee on Animal Research in the Tsinghua University.

5

6   **2.2. Synthesis of star-shaped copolymer CA-(PCL-ran-PLA)-b-PEG$_{1k}$**

7   The star-shaped copolymer CA-(PCL-*ran*-PLA)-*b*-PEG$_{1k}$ was synthesized as

8   described in the literature [2,5], including three stages of chemical reaction: Ring

9   opening polymerization of ε-caprolactone and lactide monomer initiated by cholic

10   acid, Carboxylated reaction of PEG, and Esterification reaction of CA-(PCL-*ran*-PLA)

11   and CPEG.

12   *2.2.1. Ring opening polymerization reaction*

13   D,L-lactide (2.88g, 20 mmol), ε-caprolactone (9.12 g, 80 mmol), initiator cholic

14   acid (0.41 g, 1 mmol) were weighted in a vacuum sealed tube with four drops of

15   stannous octoate as catalyst. The mixture in the sealed tube was placed in the constant

16   temperature drier at 160 ℃ and allowed to react for about 12 h. After cooling to

17   room temperature, the sealed tube was opened, and the resulting copolymers were

18   dissolved in DCM and then precipitated in excess cold ether, using methanol to

19   remove unreacted monomers. The final product, pure CA-(PCL-*ran*-PLA) was

20   collected by filtration and vacuum dried at 40 ℃ for 24 h. In addition, the linear

21   copolymer PEG$_{1k}$-*b*-(PCL-*ran*-PLA) was synthesized in the same way except the

22   initiator cholic acid was replaced by PEG.

1 *2.2.2. Carboxylated reaction of PEG*

2 PEG (M_n=1000, 10 g, 10.0 mmol), succinic anhydride (1.2 g, 12.0 mmol),

3 DMAP 1.22 g, 10.0 mmol), and TEA (1.01 g, 10.0 mmol) were dissolved in 40 mL of

4 anhydrous dioxane and stirred for 24 h at room temperature. The solvent was

5 completely evaporated with a rotary evaporator. The residue was dissolved in DCM,

6 washed with 10% hydrochloric acid and saturated brine respectively, dried by

7 anhydrous magnesium sulfate and filtered to remove unreacted succinic anhydride

8 and other substance. After filtration, the solution then precipitated in excess cold ether.

9 The final product (pure CPEG) was collected and vacuum dried at 35 ℃ for 24 h.

10 *2.2.3. Esterification reaction between CA-(PCL-ran-PLA) and CPEG*

11 Certain amounts of CA-(PCL-ran-PLA), CPEG (obtained through previous

12 reactions), dicyclohexyl carbodiimide (DCC), and DMAP were weighted in a dried

13 Schlenk tube connected to an argon-filled balloon, which can create an argon

14 atmosphere. The mixture was allowed to react by magnetic stirring under room

15 temperature for 24 h. The reaction byproduct dicyclohexylcarbodiurea (DCU) was

16 removed by filtration and then precipitated in anhydrous ether. The obtained

17 star-shaped block polymer CA-(PCL-*ran*-PLA)-*b*-PEG$_{1k}$ was purified by solvent

18 extraction using ether and benzene as a co-solvent. The final product (white powder)

19 was collected and dried in vacuo at 40 ℃.

20

21 **2.3. Characterization of star-shaped CA-(PCL-ran-PLA)-b-PEG$_{1k}$ copolymer**

22 The structure of synthesized CA-(PCL-*ran*-PLA) and

1   CA-(PCL-*ran*-PLA)-*b*-PEG$_{1k}$ was confirmed by NMR (Bruker AMX 500) with

2   CDCl$_3$ used as a solvent. Gel permeation chromatography (Waters GPC analysis

3   system with RI-G1362A refractive index detector, Milford, USA) was used to

4   measure the molecular weight and molecular weight distribution. THF was used as

5   the eluent at a flow rate of 1 ml/min to calibrate the data against polystyrene standards.

6   The thermal properties of star-shaped CA-(PCL-*ran*-PLA)-*b*-PEG$_{1k}$ were studied by

7   thermogravimetric analysis (TGA, TGA Q500 thermogravimetric analyzer, USA).

8   During TGA measurement, approximately 10 mg of copolymer sample was heated

9   from 40 ℃ to 600 ℃ at a rate of 20 ℃/min. The weight loss pattern in the

10   copolymer thermogram could be related to the composition of the polymer.

11

12   **2.4. Formulation of DTX-loaded CA-(PCL-ran-PLA)-b-PEG$_{1k}$ NPs**

13   A modified nano-precipitation method with an acetone-water system was used to

14   prepare DTX-loaded CA-(PCL-*ran*-PLA)-*b*-PEG$_{1k}$ NPs [40]. In a word, 20 mg DTX

15   powder and 200 mg CA-(PCL-*ran*-PLA)-*b*-PEG$_{1k}$ copolymer were dissolved in 16 ml

16   acetone, and then the organic solution was injected into 200 ml TPGS aqueous

17   solution (0.03%, w/v) under gentle stirring. Afterwards, the mixture was stirred at the

18   speed of 800 rpm overnight to remove acetone completely (at room temperature). The

19   resulting particles suspension was centrifuged at 15,000 rpm for 20 min (4 ℃), and

20   the precipitates were washed three times to get rid of the emulsifier and

21   unencapsulated DTX. The resulting particles were resuspended in 10 ml deionized

22   water, and placed in -80 ℃ refrigerator overnight. At last, the solid was freeze-dried

1   for two days. Drug-loaded CA-(PCL-*ran*-PLA) and PEG$_{1k}$ -*b*-(PCL-*ran*-PLA) NPs

2   were fabricated with the same method. The fluorescent coumarin-6 loaded

3   CA-(PCL-*ran*-PLA)-*b*-PEG$_{1k}$ NPs were prepared in the same way except coumarin-6

4   was encapsulated instead of DTX.

5

6   **2.5. Nanoparticles Characterization**

7   *2.5.1. Particle size, zeta potential and surface morphology*

8   For the measurement of particle size and zeta potential, the NPs were

9   resuspended in deionized water before experiments, and Malvern Mastersizer 2000

10   (Zetasizer Nano ZS90, Malvern Instruments Ltd., UK) was used in this study. The

11   data were gained with the average of three times.

12   For observation of the surface morphology of NPs, a field emission scanning

13   electron microscopy (FESEM, S-4800, Hitachi, Tokyo, Japan), operated at a 15.0 kV

14   accelerating voltage, was used in this experiment. The particles were fixed on a

15   copperplate by double-sided sticky conductive adhesives and then coated with

16   platinum layer by JCF-1300 automatic fine platinum coater to prepare samples for

17   FESEM. Transmission electron microscopy (TEM, Tecnai G2 20, FEI Company,

18   Hillsboro, Oregon, USA) was used to further observe the resultant NPs. Sample was

19   dropped onto a carbon-coated-on lacey support film and the lacey support film was

20   allowed to dry before characterization.

21   *2.5.2. Drug loading and encapsulation efficiency*

22   The drug loading content (LC) and encapsulation efficiency (EE) of DTX-loaded

1 NPs was determined by HPLC (LC 1200, Agilent Technologies, Santa Clara, CA)

2 with the same method previously published in our study [41]. 5 mg DTX-loaded NPs

3 were dissolved in 1 ml DCM under vigorous vortexing. Then the solution was

4 transferred to 5 ml of mobile phase consisting of acetonitrile and deionized water

5 (50:50, v/v). A nitrogen stream was introduced to evaporate the DCM for about 20

6 min, and then a clear solution was obtained for HPLC analysis. The flow rate of

7 mobile phase was set at 1.0 ml/min. A reverse-phase C_{18} column (150×4.6 mm, 5 μm,

8 C_{18}, Agilent Technologies, CA, USA) was used in this study, and the column effluent

9 was detected at 227 nm with a UV/VIS detector. The drug loading content and

10 encapsulation efficiency of the DTX-loaded NPs were calculated by the following

11 equations respectively [20]. Each batch was conducted in three times.

12
$$LC\ (\%) = \frac{\text{Weight of DTX in the nanoparticles}}{\text{Weight of the nanoparticles}} \times 100\%$$

13
$$EE\ (\%) = \frac{\text{Weight of DTX in the nanoparticles}}{\text{Weight of the feeding DTX}} \times 100\%$$

14 *2.5.3. In vitro drug release*

15 *In vitro* DTX release from drug-loaded nanoparticles was performed as the

16 followings. 5 mg lyophilized DTX-loaded NPs were dispersed in 5 mL

17 Phosphate-Buffered Saline (PBS, pH = 7.4, containing 0.1%w/v Tween 80) to form a

18 suspension. Tween 80 was used to raise the solubility of DTX in PBS and prevent it

19 from adhering to the tube wall. Then the suspension was transferred to a dialysis bag

20 (MWCO: 3500 Da, Spectra/Por® 6, Spectrum Laboratories, CA, USA), which was

21 immerged in 15 mL of PBS release medium in a centrifuge tube. The tube was

1 transferred into an orbital water bath and shaken at 120 rpm at 37°C. At designated

2 time intervals, 10 mL of release medium was taken out for HPLC analysis and

3 replaced with fresh PBS solution, and the tube was put back into the shaker for

4 continuous analysis. The accumulative release of drug from DTX-loaded NPs was

5 plotted against time.

6

7 **2.6. Cellular uptake of fluorescent NPs**

8 The HepG2 cells were cultivated in the chambered cover glass system in

9 Dulbecco's Modified Eagle's Medium (DMEM) supplemented with 10%

10 heat-inactivated fetal bovine serum, 100 U/ml penicillin, and 100 mg/ml streptomycin

11 in 5% CO_2 at 37 ℃. A fluorescent probe (coumarin-6) was used to replace the DTX

12 in the nanoformulation for the observation and analysis of cellular uptake of NPs [42,

13 43]. After the cells were incubated with 250 μg/ml coumarin-6 loaded

14 CA-(PCL-*ran*-PLA)-*b*-PEG_{1k} NPs at 37 °C for 4 h, the cells were rinsed with cold

15 PBS for three times and then fixed by cold methanol for 20 min. The nuclei were

16 counterstained with 4′,6-diamidino-2-phenylindole dihydrochloride (DAPI, Fluka,

17 Buche, Switzerland) for 10 min, then the stained cells were washed three times again

18 with PBS to get rid of free DAPI. In order to visualize HepG2 cells, the chambers

19 were mounted onto the confocal laser scanning microscope (CLSM, Olympus

20 Fluoview FV-1000, Tokyo, Japan) with imaging software. Images of the cells were

21 determined with a differential interference contrast channel. Nuclei of cells stained by

22 DAPI and coumarin-6 loaded NPs were recorded by the following channels: blue

1   channel with excitation at 340 nm and green channel with excitation at 485 nm.

2   For flow cytometric (FCM) assay, the HepG2 cells were incubated with 250

3   μg/ml coumarin-6 loaded CA-(PCL-*ran*-PLA), PEG$_{1k}$-*b*-(PCL-*ran*-PLA) and

4   CA-(PCL-*ran*-PLA)-*b*-PEG$_{1k}$ NPs at 37 °C for 1 h, respectively. The cells were

5   collected and washed with PBS, and the intracellular fluorescence of coumarin-6 was

6   detected by FCM after excitation at 488 nm. Fluorescence emission at 530 nm from

7   10,000 cells were collected, amplified and scaled to generate single parameter

8   histogram.

9   For the quantitative analysis, HepG2 cells (initial density of 1×10^4 cells/well)

10   were plated in 96-well plates and cultivated overnight [44, 45]. Hank's buffered salt

11   solution (HBSS) was used to equilibrate the cells at 37 ℃ for 1 h, then coumarin-6

12   loaded NPs were added at concentrations of 100, 250 and 500 μg/ml, respectively.

13   After 2 hour-incubation, the medium was removed and the wells were washed three

14   times with 50 μl cold PBS solution. At last, 50 μl 0.5% Triton X-100 in 0.2 N sodium

15   hydroxide was put into each sample well to lyse the cells.

16

17   **2.7. In vitro cell viability assay**

18   HepG2 cells were seeded in 96-well plates at the density of 5000 viable cells per

19   well, and incubated 24 h to allow cell attachment. After that, the cells were incubated

20   with DTX-loaded CA-(PCL-*ran*-PLA)-*b*-PEG$_{1k}$ NPs, PEG$_{1k}$-*b*-(PCL-*ran*-PLA) NPs

21   suspension, commercial Taxotere$^{®}$ at 0.25, 2.5, 12.5 and 25 μg/ml equivalent DTX

22   concentrations and drug-free CA-(PCL-*ran*-PLA)-*b*-PEG$_{1k}$ NPs suspension with the

1   same amount of NPs for 24, 48 and 72 h, respectively. The formulations were

2   replaced with DMEM containing MTT (5 mg/ml) at a determined time, and incubated

3   cells for an additional 4 h. Then MTT was aspirated off and DMSO was added to

4   dissolve the formazan crystals (incubated for 2 h at 37 ℃ in dark). A microplate

5   reader (Bio-Rad Model 680, UK) was used to measure absorbance at 570 nm, and

6   untreated cells were taken as control with 100% viability, while cells without addition

7   of MTT were used as blank to calibrate the spectrophotometer to zero absorbance.

8   IC_{50}, drug concentration at which inhibited of 50% cell growth, was calculated by

9   curve fitting of the cell viability data in comparison with that of the control samples.

10

11   **2.8. Anti-tumor efficacy study with xenograft tumor model**

12   HepG2 tumor cells (2×10^6 cells/mouse) in the culture medium were implanted

13   into the subcutaneous space of BALB/c nude mice (15-20 g) at right axilla and the

14   tumor growth in each mouse was observed frequently. Tumor size was measured by a

15   vernier caliper and its volume (V) was calculated as $V=d^2 \times D/2$, where d and D

16   represent for the shortest and the longest diameter of the tumor in mm, respectively.

17   Animals were closely observed for clinical signs and behavior. At the moment the

18   tumor volume reached around 50 mm^3 (designated as the 0 day), treatments were

19   performed. The mice were randomly divided into three groups (each group has 5

20   animals, *n*=5). With Saline as control, the DTX-loaded CA-(PCL-*ran*-PLA)-*b*-PEG$_{1k}$

21   NPs and Taxotere$^®$ were intraperitoneal injected at a single dose of 10 mg DTX/kg in

22   saline on days 0, 4, 8 and 12. Mice were sacrificed by cervical decapitation after 14

days' treatment. The terminal tumor weight was measured and utilized to evaluate the

antitumor activity.

2.9. Statistical methodology

All experiments were repeated at least three times unless otherwise stated. The

results are expressed as mean ± SD, and the statistical significance of all results was

determined by Student's t-test. $P < 0.05$ was considered significant.

3. Results and discussion

3.1. Synthesis and characterization of CA-(PCL-*ran*-PLA)-*b*-PEG$_{1k}$ copolymer

With Sn(Oct)$_2$ as a catalyst in bulk, the star-shaped random copolymer

CA-(PCL-*ran*-PLA) was synthesized via a ring-opening copolymerization of

ε-caprolactone (CL) and D,L-lactide (LA) initiated by multifunctional cholic acid (CA)

at 160 ℃. Studies have demonstrated that ring-opening polymerization is an efficient

method for preparing aliphatic polyesters with high molecular weights [46]. With the

help of initiators possessing hydroxyl groups, we can achieve the controlled

architectures of copolymers, such as linear, comb-like and star-shaped [47]. As shown

in Fig.1, synthesized CA-(PCL-*ran*-PLA) was connected to the carboxylated PEG

through an esterification reaction with DCC and DMAP as catalysts, ultimately

generating the three-arm CA-(PCL-*ran*-PLA)-*b*-PEG$_{1k}$ copolymer.

In order to confirm the formation of the star-shaped random copolymer, ^{1}H NMR

spectrum is recorded and the detailed assignment of the signals is shown in Fig. 2.

1   The typical signals from monomers CL and LA repeating units and CA moiety could

2   be observed in CA functionalized star-shaped polymer CA-(PCL-*ran*-PLA). ^{1}H NMR

3   (CDCl$_3$): a (δ = 5.21 ppm, LA repeating unit: -C$\underline{H}$CH$_3$), b (δ = 4.05 ppm, CL

4   repeating unit: -C$\underline{H}_2$OCO-), c (δ = 2.31 ppm, CL repeating unit: -COC$\underline{H}_2$-), d+g (δ =

5   1.55-1.70 ppm, CL repeating unit: -(C$\underline{H}_2$)$_5$- and LA repeating unit: -C$\underline{H}_3$), e (δ = 1.38

6   ppm, CL repeating unit: -(C$\underline{H}_2$)$_5$-). The successful coupling of star-shaped

7   CA-(PCL-*ran*-PLA) and CPEG was confirmed by the appearance of peak f (δ = 3.65

8   ppm, methoxyl protons of PEG: -C$\underline{H}_2$C$\underline{H}_2$O-) and peak h (δ = 3.38 ppm, methoxyl

9   protons of PEG: -OC$\underline{H}_3$) in the spectra. The ^{1}H NMR spectrum provides evidences

10   that star-shaped copolymers CA-(PCL-*ran*-PLA) and CA-(PCL-*ran*-PLA)-*b*-PEG$_{1k}$

11   with a well-defined three-branched structure were synthesized successfully. The

12   actual molecular weights (data shown in Table 1) of star-shaped copolymers

13   CA-(PCL-*ran*-PLA) and CA-(PCL-*ran*-PLA)-*b*-PEG$_{1k}$ were calculated from the peak

14   areas integral ratio of a (δ = 5.21 ppm), b (δ = 4.05 ppm) and f (δ = 3.65 ppm).

15   For the purpose of investigating the thermal properties, TGA was conducted on

16   the synthesized random copolymer CA-(PCL-*ran*-PLA)-*b*-PEG$_{1k}$. The typical thermal

17   decomposition profiles for carboxyl-terminated PEG, CA-(PCL-*ran*-PLA) and

18   CA-(PCL-*ran*-PLA)-*b*-PEG$_{1k}$ were displayed in Fig.3. The thermal decomposition

19   process of star-shaped copolymer CA-(PCL-*ran*-PLA)-*b*-PEG$_{1k}$ had two stages of

20   weight loss, whereas CA-(PCL-*ran*-PLA) and CPEG only had a single step of mass

21   loss. The combustion of a new component in the copolymer was marked by each

22   turning point: the first stage (approximately 250-380℃) should be attributed to the

1 decomposition of CA-(PCL-*ran*-PLA) segments, while the second stage

2 (approximately 380-450℃) be assigned to the decomposition of PEG segments,

3 further proving the presence of two blocks in the star-shaped copolymer

4 CA-(PCL-*ran*-PLA)-*b*-PEG$_{1k}$.

5   The molecular weights of the obtained copolymers were measured by ^{1}H NMR

6 spectra and GPC, respectively. The detailed results are presented in Table 1. For

7 star-shaped copolymers CA-(PCL-*ran*-PLA) and CA-(PCL-*ran*-PLA)-*b*-PEG$_{1k}$, the

8 M_n evaluating from ^{1}H NMR spectrum is larger than that of GPC (14,361.86 vs

9 12,045.32, 17,535.43 vs 14,972.69, respectively). This could be attributed to the

10 molecular weight estimated by GPC analysis using linear polymer as calibration.

11 Star-shaped copolymer has a smaller hydrodynamic volume than linear polymer with

12 similar molecular weight, and can hardly be expanded in solution. Furthermore, the

13 molecular weight polydispersity of the copolymer is rather narrow.

14

15 **3.2. Formulation and characterization of NPs**

16   As displayed in Fig. 4 (A), the DTX-loaded CA-(PCL-*ran*-PLA)-*b*-PEG$_{1k}$ NPs

17 was formulated by a modified nano-precipitation method with acetone as acceptable

18 solvent, which provided a facile, mild, and energy-saving pathway for drug

19 encapsulation of polymeric NPs. Random copolymers and DTX without any chemical

20 modification could be completely dissolved in acetone to generate a homogenous and

21 clear solution. The formulation process could be described as followings: When the

22 acetone solution was injected into the continuous stirred aqueous solution, the

water-insoluble DTX was immediately precipitated. In the meantime the hydrophobic

-(PCL-*ran*-PLA)- segment of the star-shaped CA-(PCL-*ran*-PLA)-*b*-PEG$_{1k}$ was also

precipitated rapidly, resulting in spontaneous formation of DTX into NPs [48]. In

order to obtain stable DTX-loaded CA-(PCL-*ran*-PLA)-*b*-PEG$_{1k}$ NPs aqueous

dispersion, the mixed solution was stirred overnight to volatilize organic solvent

acetone. Eventually, the NPs possess a hydrophilic stabilization shell (PEG segment),

a core-shell structure (hydrophobic PCL-*ran*-PLA segment) and a hydrophobic core

(entrapped DTX).

3.2.1. Size, zeta potential and surface morphology of NPs

Cellular uptake, drug release, *in vivo* pharmacokinetics and biodistribution are

closely related to particle size and surface properties [49], a dynamic light scattering

(DLS) was used in order to measure the size and size distribution of the DTX-loaded

NPs, and the data is shown in Table 2. The mean hydrodynamic size of DTX-loaded

NPs is about 90~140 nm in diameter. Within this size range, NPs can easily

accumulate in tumor vasculature under the influence of the enhanced permeability and

retention effect [50]. The average particle size of DTX-loaded

CA-(PCL-*ran*-PLA)-*b*-PEG$_{1k}$ NPs is about 95.1 nm and the polydispersity index (PDI)

value is 0.167. Compared with those of CA-(PCL-*ran*-PLA) NPs (~127.2 nm, PDI

0.203) and DTX-loaded PEG$_{1k}$-*b*-(PCL-*ran*-PLA) NPs (~140.6 nm, PDI 0.237), the

average particle size were much smaller and the size distribution were much narrower.

The data indicated that star-shaped and constrained geometry architecture of

copolymer may be attributed to small size and narrow size distribution of DTX-loaded

1 NPs, which is useful for nanomedical application. The size distribution of

2 DTX-loaded CA-(PCL-*ran*-PLA)-*b*-PEG$_{1k}$ NPs is shown in Fig.4 (B).

3 The zeta potential of DTX-loaded CA-(PCL-*ran*-PLA)-*b*-PEG$_{1k}$ NPs was

4 observed to be -8.3 mV, a slightly increase compared with that of DTX-loaded

5 PEG$_{1k}$-*b*-(PCL-*ran*-PLA) NPs (-12.5 mV) and CA-(PCL-*ran*-PLA) NPs (-20.3 mV),

6 as shown in Fig.2. The slightly negative charge of DTX-loaded

7 CA-(PCL-*ran*-PLA)-*b*-PEG$_{1k}$ NPs can reduce the undesirable clearance by the

8 reticuloendothelial system (e.g. liver) and improve the blood compatibility, thus

9 facilitating NPs accumulation at the tumor sites [51].

10 The surface morphology of DTX-loaded CA-(PCL-*ran*-PLA)-*b*-PEG$_{1k}$ NPs was

11 investigated by field emission scanning electron microscopy and transmission

12 electron microscopy. Fig. 4 illustrates the FESEM (C) and TEM (D) image of

13 DTX-loaded CA-(PCL-*ran*-PLA)-*b*-PEG$_{1k}$ NPs. The NPs seemed to have a

14 near-spherical shape with rough surface and were around 60 nm in diameter, reaching

15 a significantly smaller size than that obtained from DLS experiments. This difference

16 may be caused by a tendency of shrink and collapse while the NPs are in dry state

17 [51].

18 *3.2.2. Drug loading content and encapsulation efficiency*

19 As displayed in Table 2, both the drug loading content (LC) and encapsulation

20 efficiency (EE) of star-shaped polymer CA-(PCL-*ran*-PLA)-*b*-PEG$_{1k}$ NPs

21 (10.13±0.4%, 97.98±1.9%) and CA-(PCL-*ran*-PLA) (9.27±0.2%, 89.36±2.9%) were

22 higher than linear polymer PEG$_{1k}$-*b*-(PCL-*ran*-PLA) NPs (8.67±0.3%, 81.57±4.5%),

1 indicating the existence of a stronger binding affinity between hydrophobic DTX and

2 the star-shaped core region PCL-*ran*-PLA. In the meantime, compared with the linear

3 polymer NPs and CA-(PCL-*ran*-PLA) NPs, CA-(PCL-*ran*-PLA)-*b*-PEG$_{1k}$ NPs can

4 wrap more drugs and be more efficient in the same amount, suggesting

5 CA-(PCL-*ran*-PLA)-*b*-PEG$_{1k}$ can be a better biomaterial applied in nanotechnology

6 and drug delivery system. As shown in Fig.5, the average particle size and zeta

7 potential of the DTX-loaded NPs (redispersion in PBS) hardly changed during the

8 investigation period, i.e. the DTX-loaded NPs exhibited a good redispersion stability.

9 ***3.2.3. In vitro DTX release from NPs***

10 Fig. 6 shows the cumulative *in vitro* release profiles of DTX-loaded

11 PEG$_{1k}$-*b*-(PCL-*ran*-PLA), CA-(PCL-*ran*-PLA) and CA-(PCL-*ran*-PLA)-*b*-PEG$_{1k}$ NPs

12 in release medium (suspended in PBS containing 0.1% w/v Tween 80, pH 7.4) at

13 37 ℃ . As can be observed in the figure, the drug release from

14 CA-(PCL-*ran*-PLA)-*b*-PEG$_{1k}$ NPs was found to be 69.46% and 79.26% of the

15 encapsulated DTX in the first 7 days and after 15 days, which was much faster than

16 that of PEG$_{1k}$-*b*-(PCL-*ran*-PLA) NPs (39.82% and 45.13% in the same periods), and

17 that of CA-(PCL-*ran*-PLA) NPs (52.87% and 63.24% in the same periods),

18 demonstrating the star-shaped random polymer for nanoformulation may have faster

19 drug release rate than the linear polymer does at a similar molecular weight. The

20 fastest drug release speed of CA-(PCL-*ran*-PLA)-*b*-PEG$_{1k}$ NPs could be attributed to

21 the shorter arms and smaller size. The release profiles of DTX-loaded NPs exhibited a

22 typical biphasic release pattern: the DTX release from the PEG$_{1k}$-*b*-(PCL-*ran*-PLA)

1 NPs, CA-(PCL-*ran*-PLA) NPs and CA-(PCL-*ran*-PLA)-*b*-PEG$_{1k}$ NPs showed an

2 initial burst of 21.34%, 28.93% and 36.42% in the first day, respectively. At last the

3 cumulative drug release of NPs approached 45~80% after 15 days. This pattern could

4 be caused by drug poorly entrapped or just beneath the periphery of the NPs, while

5 the subsequent sustained release was mainly caused by the diffusion of drug which

6 was well encapsulated in the rigid core of NPs.

7

8 **3.3. Cellular uptake of fluorescent NPs by HepG2 cells**

9 In order to visualize and analyze cellular uptake of the NPs, a fluorescent probe

10 called coumarin-6 was used to represent the DTX in the NPs and confocal laser

11 scanning microscopy (CLSM) was used to observe this process and distribution of

12 NPs in cells. Fig. 7 displays CLSM images of HepG2 cells after 4 h incubation with

13 the coumarin-6 loaded CA-(PCL-*ran*-PLA)-*b*-PEG$_{1k}$ NPs suspension in the

14 Dulbecco's modified Eagle medium (DMEM) at 250 μg/ml nanoparticle

15 concentration. The images were obtained from (A) the DAPI channel (blue); (B) the

16 EGFP channel (green); (C) the overlay of the two channels. It can be seen from the

17 figure that the coumarin-6 loaded CA-(PCL-*ran*-PLA)-*b*-PEG$_{1k}$ NPs (green) were

18 closely located around the nuclei (blue, stained by DAPI), demonstrating the

19 fluorescent NPs had been internalized into the HepG2 cells.

20 The cellular internalization and sustained retention properties of the NPs were

21 demonstrated to play an important role on the therapeutic effects of the drug-loaded

22 nanoformulation [52]. For valuing the internalization and sustained retention

1   properties   of PEG_{1k}-*b*-(PCL-*ran*-PLA),   CA-(PCL-*ran*-PLA)   and

2   CA-(PCL-*ran*-PLA)-*b*-PEG_{1k} NPs, the cellular uptake efficiency of the coumarin-6

3   loaded NPs was tested through 2 h incubation. As presented in Fig. 7 (D), the cellular

4   uptake efficiency of all coumarin6-loaded NPs decreased with the increase of the

5   incubated NPs concentration from 100 to 500 μg/ml. It has been reported that NPs

6   could be internalized into the cells, but the endocytic process of NPs could be

7   influenced by particle size [53, 54]. In consistent with these reports, our data showed

8   that the cellular uptake efficiency of CA-(PCL-*ran*-PLA)-*b*-PEG_{1k} NPs was 1.83-,

9   2.17-, and 2.12-fold higher than that of PEG_{1k}-*b*-(PCL-*ran*-PLA) NPs at the incubated

10   NPs concentration of 100, 250, and 500 μg/ml, respectively. Furthermore, the cellular

11   uptake efficiency of both CA-(PCL-*ran*-PLA)-*b*-PEG_{1k} and CA-(PCL-*ran*-PLA) NPs

12   was higher than that of PEG_{1k}-*b*-(PCL-*ran*-PLA) NPs at any concentration.

13   Cellular uptake of coumarin-6 loaded NPs was also confirmed by flow

14   cytometric (FCM) assay. As shown in Fig. 7 (E), the fluorescence intensity of cells

15   treated with CA-(PCL-*ran*-PLA)-*b*-PEG_{1k} NPs was the highest, followed by that of

16   CA-(PCL-*ran*-PLA) NPs, and that of PEG_{1k}-*b*-(PCL-*ran*-PLA) NPs was the lowest

17   after 1 h incubation, further indicating that CA-(PCL-*ran*-PLA)-*b*-PEG_{1k} NPs was in

18   an appropriate size distribution easy for cellular internalization and sustained retention,

19   which could also lead to excellent therapeutic effects.

20

21   **3.4. In vitro cell viability assay**

22   For the purpose of investigating the *in vitro* cytotoxicity of DTX-loaded

1   PEG_{1k}-*b*-(PCL-*ran*-PLA) NPs, DTX-loaded CA-(PCL-*ran*-PLA)-*b*-PEG_{1k} NPs and

2   drug-free CA-(PCL-*ran*-PLA)-*b*-PEG_{1k} NPs, MTT assay was conducted in the HepG2

3   cell line compared with clinically available DTX formulation, i.e. Taxotere[®]. The

4   DTX-loaded NPs were sterilized by gamma ray to exclude any contamination before

5   suspended and cultured with HepG2 cells.

6   Fig. 8 shows the *in vitro* cell viability of HepG2 cells after 24, 48, and 72

7   hour-incubation with DTX-loaded CA-(PCL-*ran*-PLA)-*b*-PEG_{1k} NPs, DTX-loaded

8   PEG_{1k}-*b*-(PCL-*ran*-PLA) NPs and Taxotere[®] at equivalent DTX concentrations of

9   0.25, 2.5, 12.5 and 25 μg/ml, respectively. Drug-free CA-(PCL-*ran*-PLA)-*b*-PEG_{1k}

10   NPs were used in control groups. As can be concluded from the figure, no obvious

11   cytotoxic activity was observed for drug-free CA-(PCL-*ran*-PLA)-*b*-PEG_{1k} NPs at

12   various concentrations from 0.25 μg/ml to 25 μg/ml, indicating the synthesized

13   star-shaped CA-(PCL-*ran*-PLA)-*b*-PEG_{1k} copolymer could be biocompatible and

14   nontoxic to tissues and cells. The cellular viability decreased with the prolonged

15   incubation time for both Taxotere[®] and DTX-loaded NPs, exhibiting a

16   dose-dependent and time-dependent effect, especially for drug-loaded

17   CA-(PCL-*ran*-PLA)-*b*-PEG_{1k} NPs. DTX-loaded CA-(PCL-*ran*-PLA)-*b*-PEG_{1k} NPs

18   exhibited the best cytotoxicity efficacy against HepG2 cells, compared with

19   Taxotere[®] and PEG_{1k}-*b*-(PCL-*ran*-PLA) NPs. For example, the HepG2 cellular

20   viability after 72 hours incubation at the 12.5 μg/ml drug concentration was 43.96%

21   for Taxotere[®], 38.27% for PEG_{1k}-*b*-(PCL-*ran*-PLA) NPs, and 18.36% for

22   CA-(PCL-*ran*-PLA)-*b*-PEG_{1k} NPs. Furthermore, in contrast with Taxotere[®], the

1   cytotoxicity of HepG2 cell was larger than 30.36% (**p < 0.01, *n*=5) and 25.60%

2   (**p < 0.01, *n*=5) for DTX-loaded CA-(PCL-*ran*-PLA)-*b*-PEG$_{1k}$ NPs after 72 hours

3   of incubation at the drug concentration of 2.5 μg/ml and 12.5 μg/ml, respectively. The

4   cytotoxicity of drug-loaded star-shaped copolymer CA-(PCL-*ran*-PLA)-*b*-PEG$_{1k}$ NPs

5   also exhibited better cytotoxicity efficacy than HepG2 cells in comparison with

6   DTX-loaded   linear   copolymer   PEG$_{1k}$-*b*-(PCL-*ran*-PLA)   NPs,   demonstrating

7   star-shaped copolymer may have more superior performance than linear copolymer in

8   drug delivery system.

9   Drug carriers based on star-shaped polymers have a lot of advantages, such as

10   lower solution viscosity, smaller hydrodynamic radius, higher drug loading content

11   (LC) and higher drug encapsulation efficiency (EE) than that of linear polymers [20,

12   46]. In the meantime, star-shaped DTX-loaded CA-(PCL-*ran*-PLA)-*b*-PEG$_{1k}$ NPs

13   have faster drug release rate and higher cell uptake efficiency than linear

14   PEG$_{1k}$-*b*-(PCL-*ran*-PLA) NPs. Therefore it is reasonable that the *in vitro* therapeutic

15   effect of star-shaped DTX-loaded CA-(PCL-*ran*-PLA)-*b*-PEG$_{1k}$ NPs is better than

16   that of linear PEG$_{1k}$-*b*-(PCL-*ran*-PLA) NPs.

17   Table 3 lists the IC$_{50}$ values of HepG2 cells after 24, 48 and 72 hours incubation

18   with DTX formulation Taxotere®, drug-loaded PEG$_{1k}$-*b*-(PCL-*ran*-PLA) NPs and

19   CA-(PCL-*ran*-PLA)-*b*-PEG$_{1k}$ NPs. The IC$_{50}$ value, which could quantitatively

20   evaluate the *in vitro* therapeutic effects of a pharmaceutical formulation, is defined as

21   the drug inhibitory concentration needed to cause 50% tumor cell mortality in a

22   designated period. As shown in the table, the IC$_{50}$ value of DTX-loaded

1   CA-(PCL-*ran*-PLA)-*b*-PEG$_{1k}$ NPs for HepG2 cells was 10.31 μg/ml, a little higher

2   than Taxotere$^®$ after 24 hours incubation. However, the IC$_{50}$ value for HepG2 cells

3   was decreased from 7.04 to 4.25 μg/mL for Taxotere$^®$, from 4.64 to 2.30 μg/ml for

4   DTX-loaded PEG$_{1k}$-*b*-(PCL-*ran*-PLA) NPs, and from 0.456 to 0.069 μg/ml for

5   DTX-loaded CA-(PCL-*ran*-PLA)-*b*-PEG$_{1k}$ NPs after 48 and 72 hours incubation,

6   respectively. The advantages in tumor cell inhibition followed the order:

7   CA-(PCL-*ran*-PLA)-*b*-PEG$_{1k}$ NPs formulation > PEG$_{1k}$-*b*-(PCL-*ran*-PLA) NPs

8   formulation > Taxotere$^®$ formulation, thus demonstrating that the DTX-loaded NPs

9   had better *in vitro* therapeutic effects for HepG2 cells, and the star-shaped

10   CA-(PCL-*ran*-PLA)-*b*-PEG$_{1k}$ was superior to linear PEG$_{1k}$-*b*-(PCL-*ran*-PLA) as drug

11   carrier for cancer chemotherapy.

12

13   **3.5. *In vivo* anti-tumor efficacy study**

14   Considering the satisfactory *in vitro* cytotoxicity against HepG2 cells, it is

15   possible that CA-(PCL-*ran*-PLA)-*b*-PEG$_{1k}$ NPs could be developed as a promising

16   deliverable vehicle for the liver cancer chemotherapy. To further investigate the *in*

17   *vivo* anti-tumor efficacy of CA-(PCL-*ran*-PLA)-*b*-PEG$_{1k}$ NPs formulation of DTX *vs*

18   Taxotere$^®$, BALB/c nude mice were subcutaneously (s.c.) inoculated into the right

19   flank with 2×10^6 HepG2 cells in 100 μl culture medium, and the results showed that

20   95% of the mice injected developed a tumor with an average volume of ~50 mm^3

21   after one week. Then the mice were randomized into 3 groups (*n* = 5 for each group)

22   and treated with DTX-loaded CA-(PCL-*ran*-PLA)-*b*-PEG$_{1k}$ nanoformulation or

1   Taxotere[®], respectively at 10 mg/kg DTX dose at day 0, 4, 8, 12 through

2   intraperitoneal injection. Physiological saline was used as control, and the tumors size

3   of the mice was recorded every 2 days until the 14th day. After two-week's therapy,

4   all mice were sacrificed and tumors were separated from the bodies at the

5   experimental terminal.

6   The morphology of the tumors of each group is presented in Fig. 9 (A). The

7   images clearly show that the tumor size for Saline group was the largest, in-between

8   for the Taxotere[®] group, and smallest for CA-(PCL-*ran*-PLA)-*b*-PEG$_{1k}$ NPs

9   formulation group. Fig. 9 (B) shows the tumor growth surveyed in the mice after the

10   intraperitoneal injection with DTX-loaded CA-(PCL-*ran*-PLA)-*b*-PEG$_{1k}$ NPs,

11   Taxotere[®] and physiological Saline. The tumor volume for saline group increased

12   obviously during the experimental period, while tumor size for

13   CA-(PCL-*ran*-PLA)-*b*-PEG$_{1k}$ nanoformulation group was significantly inhibited. The

14   weights of the tumors in each group showed in Fig. 9 (C) also indicated the

15   advantages of the DTX-loaded CA-(PCL-*ran*-PLA)-*b*-PEG$_{1k}$ NPs *vs* Taxotere[®] in

16   suppressing tumors were significant. In summary, it can be confirmed that DTX

17   nanoformulation in the CA-(PCL-*ran*-PLA)-*b*-PEG$_{1k}$ NPs could maintain its

18   pharmacological activity and significantly inhibit the tumor growth than Taxotere[®] at

19   the same dose.

20

21   **4. Conclusions**

22   In this research, a novel system of cholic acid functionalized star-shaped

1   CA-(PCL-*ran*-PLA)-*b*-PEG$_{1k}$ NPs was developed for sustained and controlled

2   delivery of DTX applied in liver cancer therapy. The DTX-loaded

3   CA-(PCL-*ran*-PLA)-*b*-PEG$_{1k}$ NPs were prepared by a modified nano-precipitation

4   technique. The hydrodynamic size of DTX-loaded CA-(PCL-*ran*-PLA)-*b*-PEG$_{1k}$ NPs

5   was about 90 nm, much smaller than that of CA-(PCL-*ran*-PLA) and linear

6   PEG$_{1k}$-*b*-(PCL-*ran*-PLA) NPs. Compared with PEG$_{1k}$-*b*-(PCL-*ran*-PLA) and

7   CA-(PCL-*ran*-PLA) NPs, the drug loading content and encapsulation efficiency of the

8   star-shaped CA-(PCL-*ran*-PLA)-*b*-PEG$_{1k}$ NPs were improved significantly. Moreover,

9   the DTX-loaded CA-(PCL-*ran*-PLA)-*b*-PEG$_{1k}$ NPs could achieve much faster drug

10   release speed, as well as higher cellular uptake efficiency and cytotoxicity by human

11   liver carcinoma cells (HepG2). Both *in vitro* cell viability experiment and *in vivo*

12   anti-tumor efficacy demonstrated that the DTX-loaded CA-(PCL-*ran*-PLA)-*b*-PEG$_{1k}$

13   NPs exhibited significantly superior anti-tumor efficiency than linear

14   PEG$_{1k}$-*b*-(PCL-*ran*-PLA) NPs and commercially available Taxotere[®] formulation. In

15   conclusion, the star-shaped CA-(PCL-*ran*-PLA)-*b*-PEG$_{1k}$ is a novel and promising

16   biodegradable copolymer for nanoformulations applied in liver cancer treatment.

17

Acknowledgements

3

References

4

5 [1] R. Lozano, M. Naghavi,et al., *Lancet*, 2012, **380**, 2095-2128.

6 [2] Y.D. Ma, L.Q. Huang, C.X. Song, X.W. Zeng, G. Liu, L. Mei, *Polymer*, 2010, **51**,

7 5952-5959.

8 [3] Y. Mi, X. Liu, J. Zhao, J. Ding, S.S. Feng, *Biomaterials*, 2012, **33**, 7519-7529.

9 [4] J. Shi, Z. Xiao, N. Kamaly, O.C. Farokhzad, *Acc. Chem. Res.*, 2011, **44**,

10 1123-1134.

11 [5] M. Colilla, B. Gonzalez, M. Vallet-Regi, *Biomater. Sci.*, 2013, **1**, 114-134.

12 [6] M. Sinn Aw, M. Kurian, D. Losic, *Biomater. Sci.*, 2014, **2**, 10-34.

13 [7] E. Wagner, *Biomater. Sci.*, 2013, **1**, 804-809.

14 [8] W.E. Bawarski, E. Chidlowsky, D.J. Bharali, S.A. Mousa, Emerging

15 nanopharmaceuticals, *Nanomed-Nanotechnol*, 2008, **4**, 273-282.

16 [9] D.B. Buxton, *Nanomedicine-Uk*, 2009, **4**, 331-339.

17 [10] H. Onyuksel, E. Jeon, I. Rubinstein, *Cancer Lett.*, 2009, **274**, 327-330.

18 [11] Y.Q. Zhang, L. Tang, L.L. Sun, J.B. Bao, C.X. Song, L.Q. Huang, K.X. Liu, Y.

19 Tian, G. Tian, Z. Li, H.F. Sun, L. Mei, *Acta Biomater.*, 2010, **6**, 2045-2052.

20 [12] L. Mei, Z.P. Zhang, L.Y. Zhao, L.Q. Huang, X.L. Yang, J.T. Tang, S.S. Feng, *Adv.*

21 *Drug Deliv. Rev.*, 2013, **65**, 880-890.

1   [13] J. Wang, K. Yao, C. Wang, C. Tang, X. Jiang, *J. Mater. Chem. B*, 2013, **1**,

2   2324-2332.

3   [14] Y. Yue, C. Wu, *Biomater. Sci.*, 2013, **1**, 152-170.

4   [15] B.H. Tan, H. Hussain, Y.W. Leong, T.T. Lin, W.W. Tjiu, C. He, *Polym. Chem.*,

5   2013, **4**, 1250-1259.

6   [16] L.Q. Huang, H.B. Chen, Y. Zheng, X.S. Song, R.Y. Liu, K.X. Liu, X.W. Zeng, L.

7   Mei, *Integr. Biol.*, 2011, **3**, 993-1002.

8   [17] Y. Wan, Z. Gan, Z. Li, *Polym. Chem.*, 2014, **5**, 1720-1727.

9   [18] Y. Yang, J. Bugno, S. Hong, *Polym. Chem.*, 2013, **4**, 2651-2657.

10 [19] V. Delplace, P. Couvreur, J. Nicolas, *Polym. Chem.*, 2014, **5**, 1529-1544.

11 [20] W. Tao, X. Zeng, T. Liu, Z. Wang, Q. Xiong, C. Ouyang, L. Huang, L. Mei, *Acta

12 Biomater.*, 2013, **9**, 8910-8920.

13 [21] L. Mei, Z. Zhang, S.S. Feng, *J. Control. Release*, 2013, **172**, e55.

14 [22] Z. Yue, Z. You, Q. Yang, P. Lv, H. Yue, B. Wang, D. Ni, Z. Su, W. Wei, G. Ma, *J.

15 Mater. Chem. B*, 2013, **1**, 3239-3247.

16 [23] K. Fujii, J. Nagai, T. Sawada, R. Yumoto, M. Takano, *Bioconjugate Chem.*, 2009,

17 **20**, 1553-1558.

18 [24] S.M. Kelleher, Z. Zhang, A. Lobus, C. Strehmel, M.C. Lensen, *Biomater. Sci.*,

19 2014, **2**, 410-418.

20 [25] J. Wang, K. Yao, C. Wang, C. Tang, X. Jiang, *J. Mater. Chem. B*, 2013, **1**,

21 2324-2332.

22 [26] B. Newland, E. Dowd, A. Pandit, *Biomater. Sci.*, 2013, **1**, 556-576.

1 [27] Z. Mao, X. Zhou, C. Gao, *Biomater. Sci.*, 2013, **1**, 896-911..

2 [28] C.M. Yang, L.Q. Jiang, S.J. Bu, L.H. Zhang, X.J. Xie, Q.G. Zeng, D.W. Zhu, Y.

3 Zheng, *J. Biomed. Nanotechnol.*, 2013, **9**, 1617-1623.

4 [29] T. Zou, S.X. Cheng, X.Z. Zhang, R.X. Zhuo, *J. Biomed. Mater. Res. B Appl.*

5 *Biomater.*, 2007, **82**, 400-407.

6 [30] H.L. Fu, L. Yu, H. Zhang, X.Z. Zhang, S.X. Cheng, R.X. Zhuo, *J. Biomed. Mater.*

7 *Res. A*, 2007, **81**, 186-194.

8 [31] C.V. Synatschke, F.A. Plamper, A.H.E. Muller, *Nachr. Chem.*, 2013, **61**,

9 1008-1012.

10 [32] M.Q. Lv, Y. Shi, W.T. Yang, Z.F. Fu, *J. Appl. Polym. Sci.*, 2013, **128**, 332-339.

11 [33] A. Swinarew, B. Piekarnik, Z. Grobelny, A. Stolarzewicz, J. Simokaitiene, E.

12 Andrikaityte, J.V. Grazulevicius, *Macromol. Symp.*, 2011, **308**, 8-11.

13 [34] A.J. Inglis, P. Pierrat, T. Muller, S. Brase, C. Barner-Kowollik, *Soft Matter.*, 2010,

14 **6**, 82-84.

15 [35] D.G. Kim, H.S. Sohn, S.K. Kim, A. Lee, J.C. Lee, *J. Polym. Sci. Pol. Chem.*,

16 2012, **50**, 3618-3627.

17 [36] L.M. de Espinosa, M. Winkler, M.A.R. Meier, *Macromol. Rapid Comm.*, 2013,

18 **34**, 1381-1386.

19 [37] D. Ma, Z.H. Liu, Q.Q. Zheng, X.Y. Zhou, Y. Zhang, Y.F. Shi, J.T. Lin, W. Xue,

20 *Macromol. Rapid Comm.*, 2013, **34**, 548-552.

21 [38] M.R. Nabid, S.J.T. Rezaei, R. Sedghi, H. Niknejad, A.A. Entezami, H.A.

22 Oskooie, M.M. Heravi, *Polymer*, 2011, **52**, 2799-2809.

[39] T.H. Li, R.Y. Han, M.Z. Wang, C.B. Liu, X.B. Jing, Y.B. Huang, *Macromol. Biosci.*, 2011, **11**, 1570-1578.

[40] P.M. Valencia, M.H. Hanewich-Hollatz, W.W. Gao, F. Karim, R. Langer, R. Karnik, O.C. Farokhzad, *Biomaterials*, 2011, **32**, 6226-6233.

[41] L. Mei, Y.Q. Zhang, Y. Zheng, G. Tian, C.X. Song, D.Y. Yang, H.L. Chen, H.F. Sun, Y. Tian, K.X. Liu, Z. Li, L.Q. Huang, *Nanoscale Res. Lett.*, 2009, **4**, 1530-1539.

[42] K.L. Hu, J.W. Li, Y.H. Shen, W. Lu, X.L. Gao, Q.Z. Zhang, X.G. Jiang, *J. Control. Release*, 2009, **134**, 55-61.

[43] S. Fokong, B. Theek, Z.J. Wu, P. Koczera, L. Appold, S. Jorge, U. Resch-Genger, M. van Zandvoort, G. Storm, F. Kiessling, T. Lammers, *J. Control. Release*, 2012, **163**, 75-81.

[44] Y.H. Loo, C.L. Grigsby, Y.J. Yamanaka, M.K. Chellappan, X. Jiang, H.Q. Mao, K.W. Leong, *J. Control. Release*, 2012, **160**, 48-56.

[45] J.X. Ding, C.S. Xiao, Y.C. Li, Y.L. Cheng, N.N. Wang, C.L. He, X.L. Zhuang, X.J. Zhu, X.S. Chen, *J. Control. Release*, 2013, **169**, 193-203.

[46] X. Zeng, W. Tao, L. Mei, L. Huang, C. Tan, S.S. Feng, *Biomaterials*, 2013, **34**, 6058-6067.

[47] H. Claesson, E. Malmstrom, M. Johansson, A. Hult, *Polymer*, 2002, **43**, 3511-3518.

[48] M.M. Yallapu, B.K. Gupta, M. Jaggi, S.C. Chauhan, *J. Colloid Interf. Sci.*, 2010, **351**, 19-29.

[49] E. Csiszar, E. Fekete, A. Toth, E. Bandi, B. Koczka, I. Sajo, *Carbohyd. Polym.*,

1   2013, **94**, 927-933.

2   [50] H. Maeda, *P. Jpn. Acad. B-Phys.*, 2012, **88**, 53-71.

3   [51] C.N. Zhang, W. Wang, T. Liu, Y.K. Wu, H. Guo, P. Wang, Q. Tian, Y.M. Wang, Z.

4   Yuan, *Biomaterials*, 2012, **33**, 2187-2196.

5   [52] A. Vollrath, D. Pretzel, C. Pietsch, I. Perevyazko, S. Schubert, G.M. Pavlov, U.S.

6   Schubert, *Macromol. Rapid Commun.*, 2012, **33**, 1791-1797.

7   [53] X. Duan, Y. Li, *Small*, 2013, **9**, 1521-1532.

8   [54] Y. Liu, M.K. Shipton, J. Ryan, E.D. Kaufman, S. Franzen, D.L. Feldheim, *Anal.*

9   *Chem.*, 2007, **79**, 2221-2229.

10

11

12

13

14

15

16

17

18

19

20

21

22

1   **Appendix**

2   Abbreviation

| Abbreviation	Description
^{1}H NMR	Proton nuclear magnetic resonance
GPC	Gel permeation chromatography
TGA	Thermogravimetric analysis
DLS	Dynamic light scattering
FESEM	Field emission scanning electron microscopy
TEM	Transmission electron microscopy
CLSM	Confocal laser scanning microscope
FCM	Flow cytometric
HPLC	High performance liquid chromatography
LC	Loading content
EE	Encapsulation efficiency
PDI	Polydispersity index
CA	Cholic acid
PCL	Poly (ε-caprolactone)
PLA	Poly(lactide)
PEG	Poly(ethylene glycol)
DTX	Docetaxel
EPR	Enhanced permeability and retention
SCID	Severe combined immunodeficient
DCC	1,3-diisopropylcarbodiimide
DCU	Dicyclohexylcarbodiurea
DMAP	4-(dimethylamino)pyridine
MTT	3-(4,5-Dimethylthiazol-2-yl)-2,5-Diphenyltetrazolium Bromide
DAPI	4′,6-diamidino-2-phenylindole dihydrochloride
HBSS	Hank's buffered salt solution
DMEM	Dulbecco's Modified Eagle's Medium

3

4

5

6

7

8

9
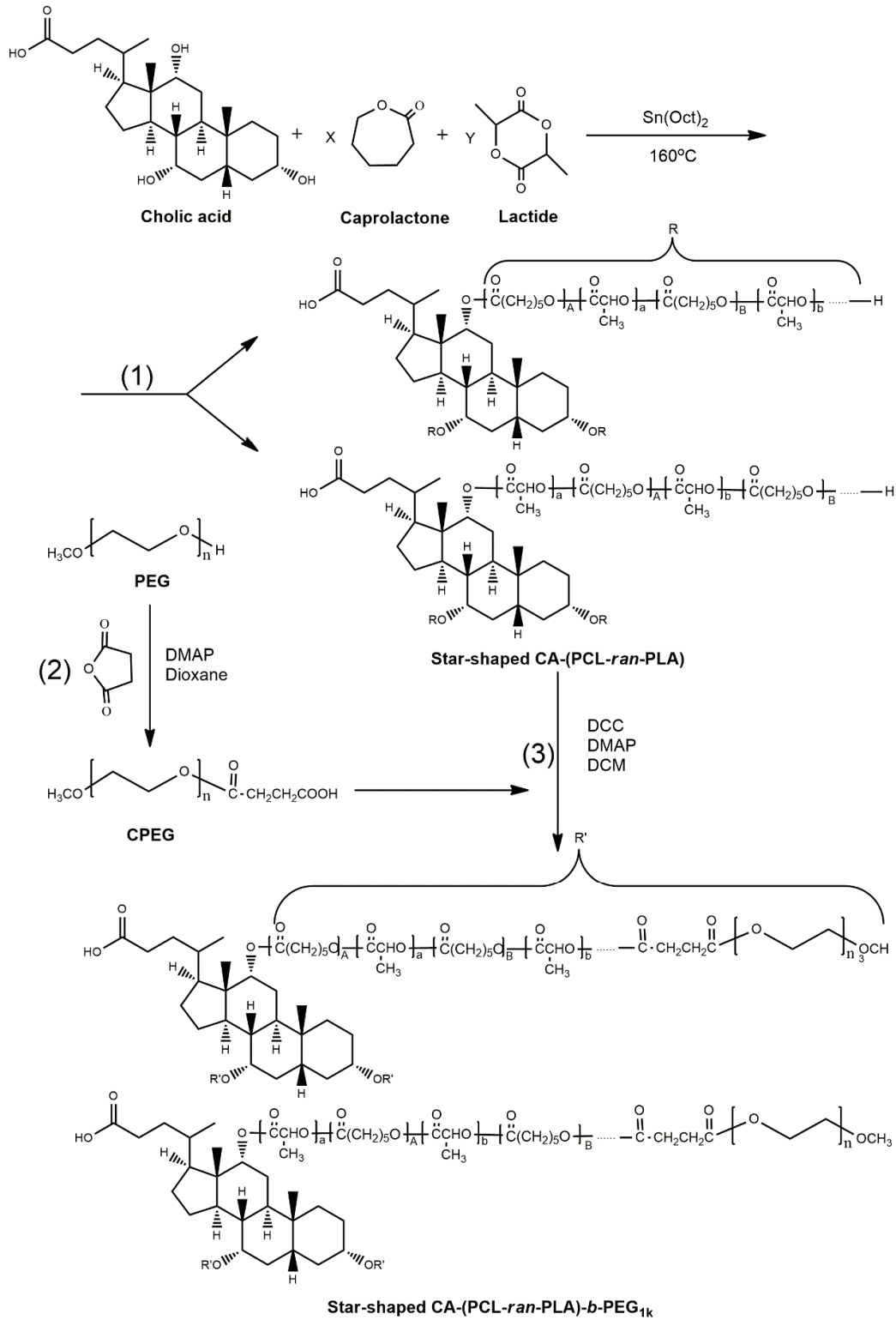
1

2   **Fig.1.** Schematic diagram of synthesis of star-shaped CA-(PCL-*ran*-PLA)-*b*-PEG$_{1k}$
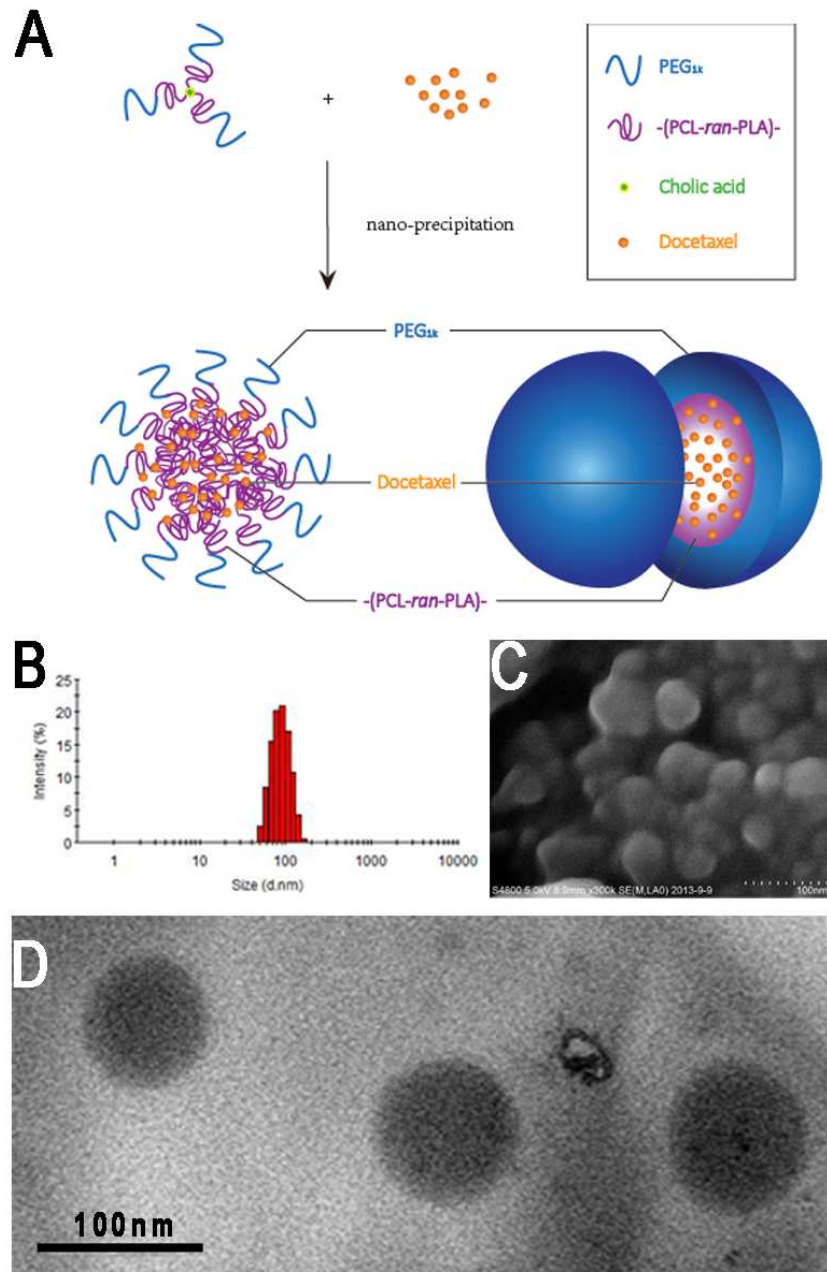
3   random copolymer.
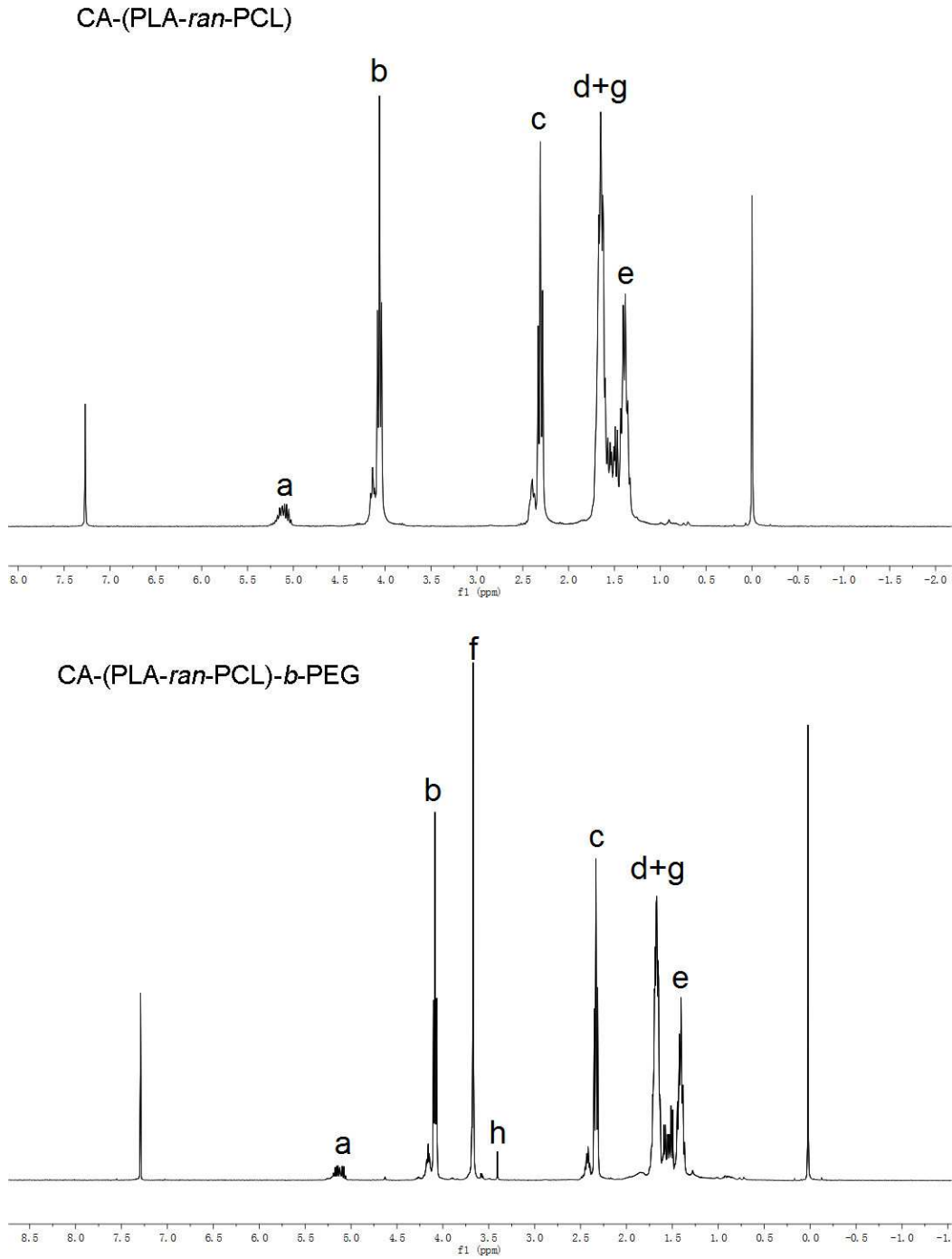
Fig.2. Typical ¹H NMR spectra of copolymer CA-(PCL-*ran*-PLA) and CA-(PCL-*ran*-PLA)-*b*-PEG$_{1k}$.
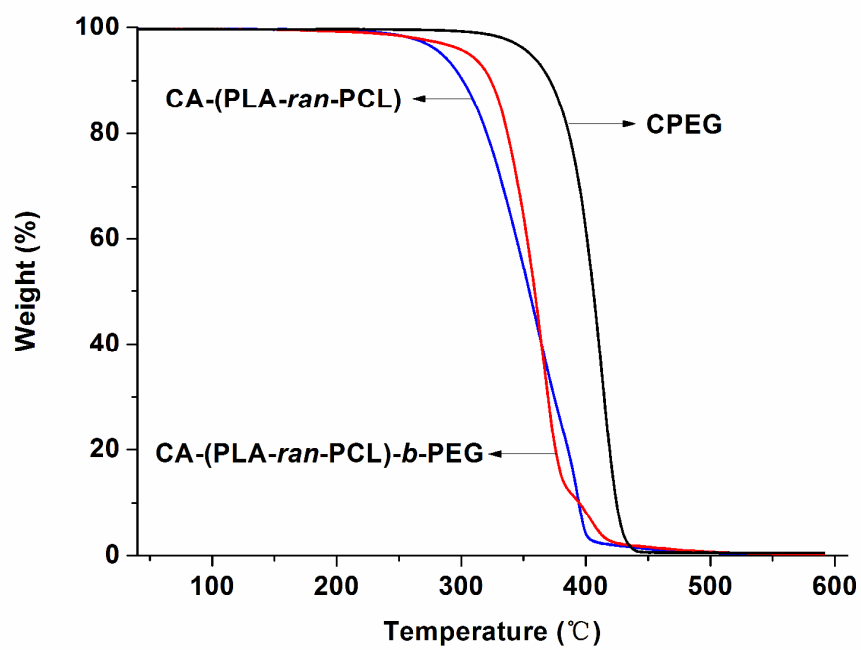
1

2   **Fig. 3.** Thermogravimetric analysis of CPEG, CA-(PCL-*ran*-PLA) and

3   CA-(PCL-*ran*-PLA)-*b*-PEG$_{1k}$ copolymers.

4

1

2 **Fig. 4.** (A) Schematic representation of technique for preparation of DTX-loaded

3 CA-(PCL-*ran*-PLA)-*b*-PEG$_{1k}$ NPs; (B) Dynamic light scattering size distribution of

4 DTX-loaded CA-(PCL-*ran*-PLA)-*b*-PEG$_{1k}$ NPs; (C) Field emission scanning electron

5 microscopy image of DTX-loaded CA-(PCL-*ran*-PLA)-*b*-PEG$_{1k}$ NPs (scale bar is 100

6 nm); (D) Transmission electron microscopy image of DTX-loaded
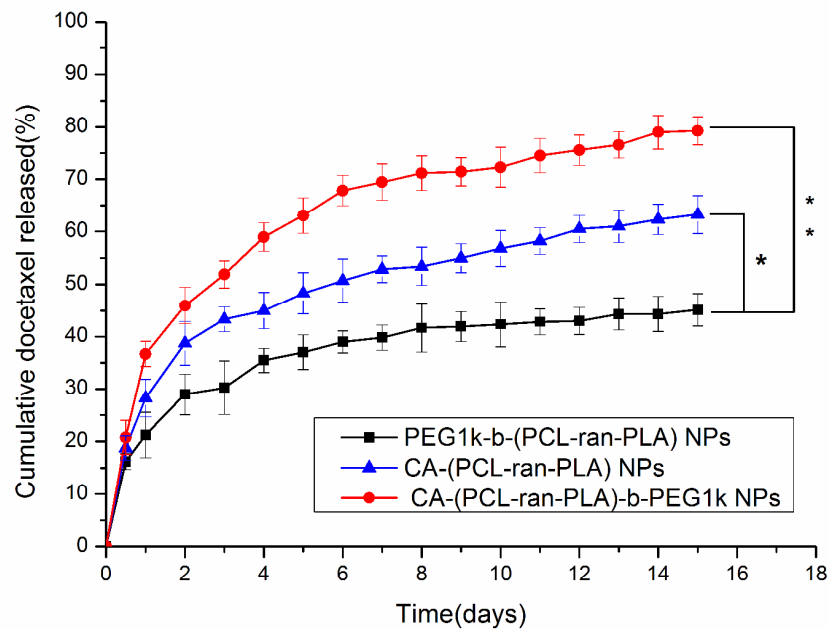
7 CA-(PCL-*ran*-PLA)-*b*-PEG$_{1k}$ NPs(scale bar is 100 nm).

1
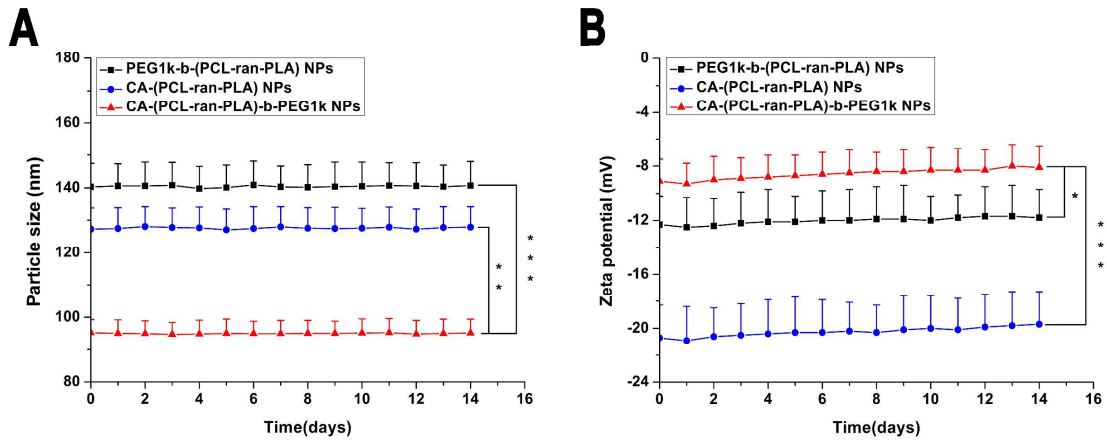
2

3 **Fig. 5.** *In vitro* stability of DTX-loaded NPs: (A) The size distribution and (B) The

4 zeta potential of DTX-loaded PEG$_{1k}$-*b*-(PCL-*ran*-PLA), CA-(PCL-*ran*-PLA) and

5 CA-(PCL-*ran*-PLA)-*b*-PEG$_{1k}$ NPs for two-week storage at 4 °C (*p < 0.05, **p <
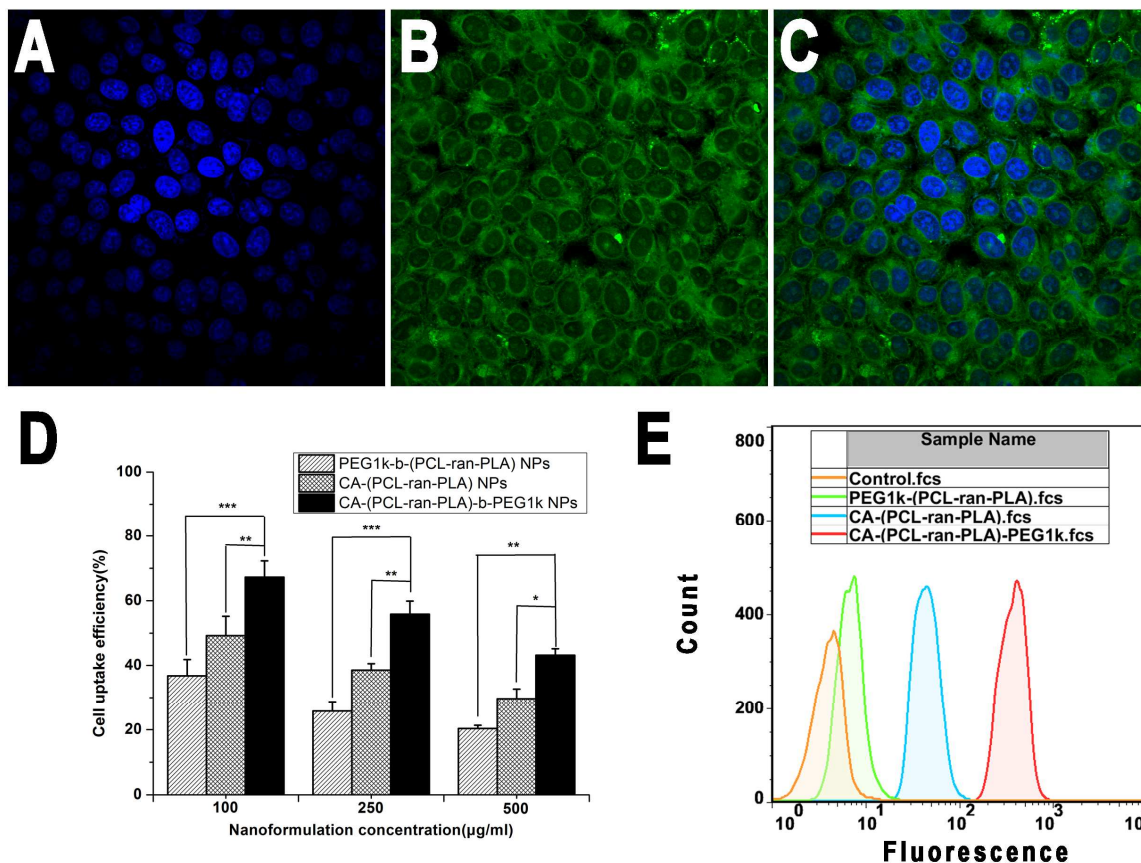
6 0.01, ***p < 0.001, n = 3).

7

8

9 **Fig. 6.** The *in vitro* release profiles of DTX-loaded PEG$_{1k}$-*b*-(PCL-*ran*-PLA) NPs,
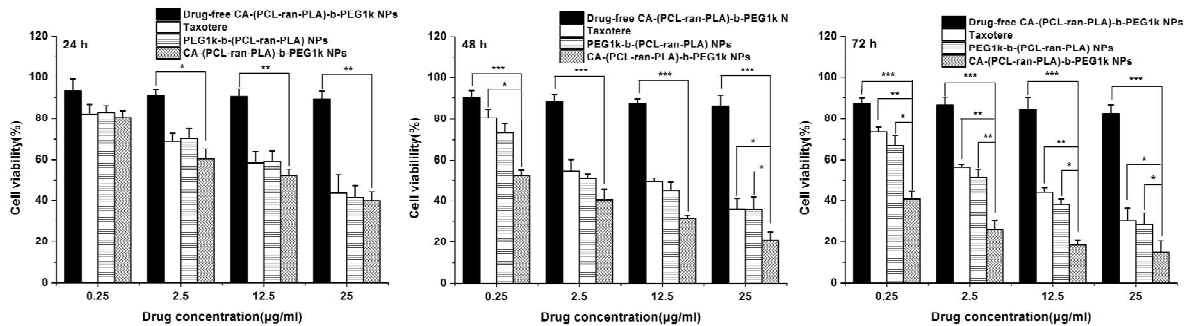
1   CA-(PCL-*ran*-PLA) NPs and CA-(PCL-*ran*-PLA)-*b*-PEG$_{1k}$ NPs at 37°C (*p < 0.05,

2   **p < 0.01, n = 5).

3

4

5   **Fig. 7.** Confocal laser scanning microscope images of HepG2 cells after 4 h

6   incubation with coumarin-6 loaded CA-(PCL-*ran*-PLA)-*b*-PEG$_{1k}$ NPs at 37 ℃. The

7   cells were stained by DAPI (blue) and the coumarin-6 loaded

8   CA-(PCL-*ran*-PLA)-*b*-PEG$_{1k}$ NPs are green. The cellular uptake was visualized by

9   overlaying images obtained by DAPI filter and EGFP filter: (A) image from DAPI

10   channel; (B) image from EGFP channel; (C) image from combined DAPI channel and

11   EGFP channel. (D) Cellular uptake efficiency of coumarin-6 loaded NPs (*p < 0.05,

12   **p < 0.01, ***p < 0.001, n = 5). (E) FCM histograms for coumarin-6 loaded NPs on

1   HepG2 cells after 1 h incubation.

2

4   **Fig. 8.** Viability of HepG2 cells incubated with DTX-loaded

5   CA-(PCL-*ran*-PLA)-*b*-PEG$_{1k}$ NPs in comparison with that of Taxotere[®] at the same

6   DTX does and that of PEG$_{1k}$-*b*-(PCL-*ran*-PLA) NPs, drug-free
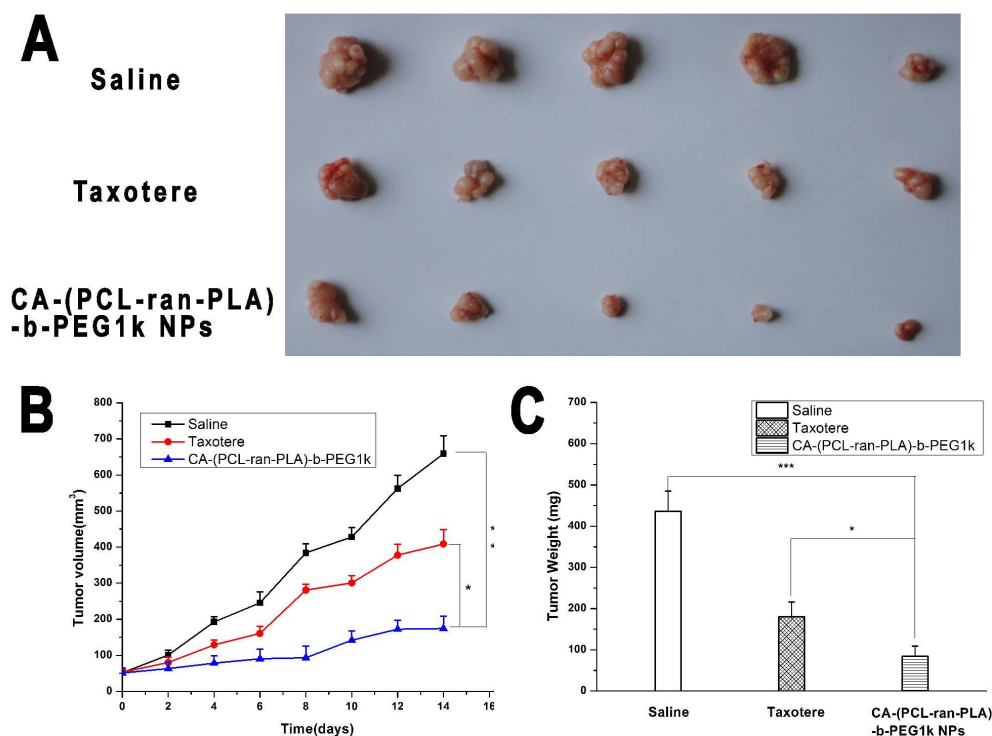
7   CA-(PCL-*ran*-PLA)-*b*-PEG$_{1k}$ NPs with the same amount of NPs. Compared with

8   Taxotere[®] and drug-loaded PEG$_{1k}$-*b*-(PCL-*ran*-PLA) NPs, significant reduction in cell

9   number for drug-loaded CA-(PCL-*ran*-PLA)-*b*-PEG$_{1k}$ NPs could be observed (*p <

10   0.05, **p < 0.01, ***p < 0.001, n = 5).

11

Biomaterials Science

1

2 **Fig. 9.** Anti-tumor efficacy of the DTX-loaded CA-(PCL-*ran*-PLA)-*b*-PEG$_{1k}$ NPs,

3 Taxotere[®] and saline on the BALB/c nude mice bearing HepG2 cells: (A) Images of

4 the tumors in each group taken out from the sacrificed mice at the end point of

5 research; (B) Tumor-growth curve of SCID mice after intraperitoneal injection with

6 DTX-loaded CA-(PCL-*ran*-PLA)-*b*-PEG$_{1k}$ NPs, Taxotere[®] and saline (*$p < 0.05$, **$p

7 < 0.01$, n=5); (C) Tumor weight of each group taken out from the sacrificed mice at

8 the end of the study. Compared with saline and Taxotere[®] groups, significant

9 reduction in tumor weight for CA-(PCL-*ran*-PLA)-*b*-PEG$_{1k}$ NPs could be observed

10 (*$p < 0.05$, ***$p < 0.001$, n = 5).

11

12

13

1   **Table 1**

2   Molecular   weights   of   star-shaped   copolymers   CA-(PCL-*ran*-PLA)   and

3   CA-(PCL-*ran*-PLA)-*b*-PEG$_{1k}$, linear copolymer PEG$_{1k}$-*b*-(PCL-*ran*-PLA).

Sample	M_n (NMR[a])	M_n (GPC[b])	M_w (GPC[b])	PDI[c]
CA-(PCL-*ran*-PLA)	14,361.86	12,045.32	15,177.47	1.26
CA-(PCL-*ran*-PLA)-*b*-PEG$_{1k}$	17,535.43	14,972.69	17,816.68	1.19
PEG$_{1k}$-*b*-(PCL-*ran*-PLA)	18,142.09	18,376.71	22,602.07	1.23

4   a Determined by ^{1}H NMR.

5   b Determined by gel permeation chromatography.

6   c Polydispersity index (M_w/M_n) determined by gel permeation chromatography.

7   M_n: Number-average molecular weight.

8   M_w: Weight-average molecular weight.

9

10 **Table 2**

11 Characterization of DTX-loaded NPs.

Polymer	Size (nm)	PDI	ZP (mV)	LC (%)	EE (%)
PEG$_{1k}$-*b*-(PCL-*ran*-PLA)	140.6 ± 7.2	0.237	-12.5± 2.1	8.67±0.3	81.57±4.5
CA-(PCL-*ran*-PLA)	127.2 ± 6.1	0.203	-20.3 ± 2.5	9.27±0.2	89.36±2.9
CA-(PCL-*ran*-PLA)-*b*-PEG$_{1k}$	95.1 ± 4.3	0.167	-8.3 ± 1.6	10.13±0.4	97.98±1.9

12 PDI = Polydispersity index, ZP = Zeta potential, LC = Loading content, EE =

13 Encapsulation efficiency, *n* = 3.

14

15 **Table 3**

16 IC$_{50}$ values of DTX formulation in the Taxotere[®], PEG$_{1k}$-*b*-(PCL-*ran*-PLA) NPs and

17 CA-(PCL-*ran*-PLA)-*b*-PEG$_{1k}$ NPs on HepG2 cells following 24, 48 and 72 hours
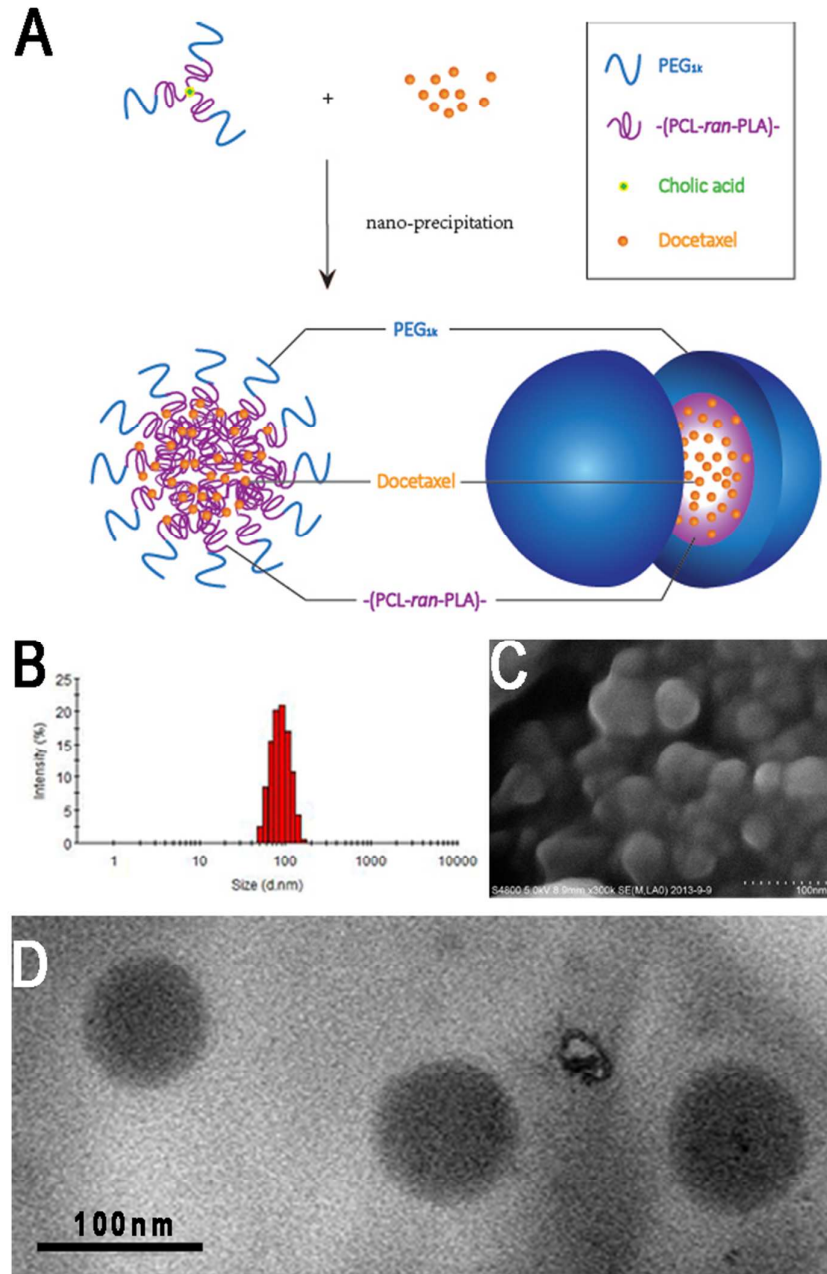
18 incubation (*n*=5).

Incubation time (h)	IC$_{50}$ (µg/mL)		
	Taxotere[®]	PEG$_{1k}$-*b*-(PCL-*ran*-PLA) NPs	CA-(PCL-*ran*-PLA)-*b*-PEG$_{1k}$ NPs
24	19.76 ± 1.83	18.63 ± 1.61	10.31 ± 1.54
48	7.04 ± 0.48	4.64 ± 0.52	0.456 ± 0.36
72	4.25 ± 0.43	2.30 ± 0.17	0.069 ± 0.05

19

20

21

Graphical Abstract

The DTX-loaded CA-(PCL-*ran*-PLA)-*b*-PEG$_{1k}$ NPs were prepared by a modified nano-precipitation method and had a near-spherical shape. These DTX-loaded NPs have great potential as drug delivery nanocarriers for cancer therapy.